analytical chemistry

pubs.acs.org/ac Article

Nitrogen-Doped Graphdiyne as a Robust Electrochemical Biosensing Platform for Ultrasensitive Detection of Environmental Pollutants

Kai Niu, Juan Gao, Lingxia Wu, Xianbo Lu,* and Jiping Chen

Cite This: *Anal. Chem.* 2021, 93, 8656−8662 Read Online

ACCESS | Metrics & More | Article Recommendations | Supporting Information

ABSTRACT: Owing to its unique chemical structure, natural pores, high structure defects, good surface hydrophilicity and biocompatibility, and favorable electrical conductivity, nitrogen-doped graphdiyne (NGDY) has been attracting attention in the application of electrochemical sensing. Taking advantage of these fascinating electrochemical properties, for the first time, two types of electrochemical enzymatic biosensors were fabricated for the respective detection of organophosphorus pesticides (OPs) and phenols based on the immobilization of acetylcholinesterase or tyrosinase with NGDY. Results revealed that the sensitivities of the NGDY-based enzymatic biosensors were almost twice higher than that of the matching biosensor in the absence of NGDY, proving that NGDY plays a vital role in immobilizing the enzymes and improving the performance of the fabricated biosensors. The effects of nitrogen doping on improving the biosensing performance were studied in depth. Graphitic N atoms can enhance the electrical conductivity, while imine N and pyridinic N can help to adsorb and accumulate the substance molecules to the electrode surface, all of which contribute to the significantly improved performance. Furthermore, these two types of biosensors also demonstrated excellent reproducibility, high stability, and good recovery rate in real environmental samples, which showed a valuable way for the rapid detection of OPs and phenols in the environment. With these excellent performances, it is strongly anticipated that NGDY has tremendous potential to be applied to many other biomedical and environmental fields.

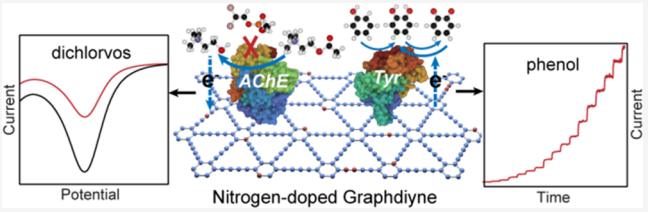

In recent decades, organophosphorus pesticides (OPs) have been used extensively to eradicate insects in agricultural areas all over the world.[1] OPs are an example of a strictly regulated toxic compound that can have harmful effects on humans and most animals even when the residues are in very small amounts. The toxic effects of OPs have the ability to inhibit the catalysis function of acetylcholinesterase (AChE), which causes interruption of neurotransmitter transmission and eventually results in death. As another essential environmental pollutant, phenolic chemicals have been extensively spread in the environment. Phenols and phenolic derivatives have been commonly used for the manufacture of different chemicals, including pesticides, plastics, and pharmaceutical products.[2] Most phenolic derivatives are endocrine-disrupting chemicals, which can cause neurotoxicity, carcinogenicity, and developmental and behavioral disorders.[3] Consequently, it is crucial to develop simple techniques for the rapid and accurate detection of OPs and phenols in the environment.

Currently, traditional analytical methods such as high-performance liquid chromatography,[4] gas chromatography−mass spectrometry,[5] and liquid chromatography−mass spectrometry[6] can provide high selectivity and good sensitivity for OP and phenol detection. These methods always require a long time for analysis, expensive equipment, a large amount of organic solvents, and highly qualified technicians, which consequently limit their further development in different fields. Fortunately, the electrochemical enzyme biosensor is an ideal analytical tool and an effective alternative to traditional methods, which enables the rapid and accurate detection of these compounds in the environment. For most OPs, common detection using an electrochemical enzyme biosensor is a kind of an indirect method, which depends on the inhibition effect of AChE, while for phenol detection, a direct electrochemical analysis of enzymatic products of tyrosinase (Tyr) was used. In order to improve the performance (sensitivity, limit of detection, stability, reliability, etc.) of the biosensor, the development has mainly focused on the fabrication and modification of electrodes with different nanomaterials, such as graphene,[7] carbon nanotubes,[8] transition-metal dichalcogenides,[9] transition-metal carbides (MXene),[10] and 2D pnictogens.[11] Carbon-based nanomaterials are the most widely used among the above nanomaterials due to their promising physical and chemical properties.

Received: April 27, 2021
Accepted: June 1, 2021
Published: June 10, 2021

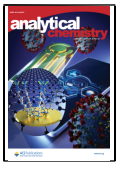

https://doi.org/10.1021/acs.analchem.1c01800
Anal. Chem. 2021, 93, 8656−8662

Numerous carbon-based nanomaterials have been found in recent decades with the development of science, such as 0D fullerene, 1D carbon nanotubes, and 2D graphene. Graphdiyne (GDY), as a new form of a carbon allotrope, comprises both sp and sp^2 hybridized carbon atoms. Compared with conventional graphene (consisting of sp^2 hybridized carbon atoms), GDY possesses natural nanopores, good surface hydrophilicity,[12] richer carbon chemical bonds, and enhanced surface functional modification capability[13] and can be easily prepared under mild conditions,[14] which are of great significance for using it as an electrode material. Due to its natural pores, high charge carrier mobility, and outstanding electronic conductivity, GDY shows outstanding performance in many fields, such as energy storage,[15] DNA detection,[16] optoelectronics,[17] and catalyst.[18] Doping GDY with heteroatoms, especially the nitrogen atom,[19−21] has proved to be an effective method to regulate the electronic characteristics and offer more active sites in the GDY carbon network, thus producing new phenomena and unexpected properties. Compared with GDY, nitrogen-doped GDY (NGDY) has improved electronic conductivity, enhanced ionic binding capability, and a significantly elevated electrochemical catalysis activity, which have greatly improved the performance of NGDY as a lithium storage material and an oxygen reduction reaction catalyst.[20,22,23] It is very attractive to explore the electrochemical sensing applications of NGDY due to its outstanding electrochemical properties. The introduction of nitrogen atoms in the carbon material can bring higher surface hydrophilicity and biocompatibility, which is one of the key advantageous factors for the immobilization of enzymes.[24] Taken together, all of these properties suggest that NGDY has enormous potential to be a universal platform for the electrochemical enzyme biosensors. Unfortunately, up to now, no progress has been made in the application of NGDY in electrochemical biosensors and environmental monitoring.

In this work, NGDY was demonstrated as an efficient biosensing platform for enzyme immobilization and biosensor fabrication. NGDY was first prepared by postheating the wet-chemical-synthesized GDY with NH_3. The unique features of the resulting NGDY include a large surface area with three-dimensional porous structures and a highly π-conjugated framework due to nitrogen doping. Then, two types of electrochemical enzymatic biosensors were fabricated for the respective detection of dichlorvos and phenols based on the immobilization of AChE or tyrosinase with NGDY. It is interesting to note that these two kinds of biosensors based on NGDY demonstrated a significantly improved biosensing performance, that is, the sensitivities were about twice higher than those of biosensors without NGDY. The possible mechanism of improving the performance was studied and discussed in depth. NGDY is evidenced to play a vital role in immobilizing enzymes and improving the performance of the fabricated biosensors, which have enormous potential applications in biomedical analysis, environmental pollutant detection, etc.

Experimental Section. Chemicals and Apparatus. AChE from *Electrophorus electricus*, tyrosinase (Tyr) from mushroom, acetylthiocholine chlorine, bovine serum albumin (BSA), glutaraldehyde (25%), and dichlorvos were purchased from Sigma (USA). Copper (Cu) foil was obtained from Sinopharm Chemical Reagent Co., Ltd. Tetrabutylammonium fluoride, pyridine, and tetrahydrofuran were obtained from Alfa Aesar (USA). AChE was dissolved in 2.5% BSA (w/v) for preservation. To obtain ultrapure water, a Milli-Q purification system (Millipore, MA, USA) with a resistivity of 18 MΩ·cm was used. Scanning electron microscopy (SEM) images were collected using a field emission scanning electron microscope JSM-7800F (JEOL, Japan). Transmission electron microscopy (TEM) images were recorded using a TEM JEM-2100 (JEOL, Japan) instrument. Raman spectra were recorded at room temperature using a Senterra (Bruker Optics, Germany) with a laser excitation from an Ar laser at a wavelength of 532 nm. The powder X-ray diffraction (XRD) spectra were obtained using a Bruker D8 Advance diffractometer (Germany) with Cu Kα radiation. The pore size distribution and surface area were calculated from nitrogen adsorption−desorption measurements, applying the Barrett−Joyner−Halenda and the Brunauer−Emmett−Teller (BET) methods using a Quantachrome Autosorb gas-sorption system at 77 K. The X-ray photoelectron spectroscopy (XPS) measurement was performed with a Thermo Fisher ESCALAB XI+ X-ray photoelectron spectrometer using Al Kα radiation as the excitation source. The binding energies collected in the XPS analysis were calibrated with reference to C 1s (284.8 eV).

Preparation of NGDY. The GDY films were prepared on the surface of copper using a cross-coupling reaction according to a previous study.[25] Then, the samples of GDY powder were placed in a tube furnace, holding the furnace tube under an NH_3 gas flow. After 10 min, the furnace was steadily heated to 300 °C within 60 min and then to 500 °C within 100 min; then, the furnace temperature was held at 500 °C for 6 h. Finally, the black NGDY powder was collected through centrifugation and drying in a vacuum oven at 50 °C for 12 h.

Fabrication of the Enzyme-Based Biosensor. The enzymatic biosensor was fabricated as schematically shown in Scheme 1 by the consecutive deposition of NGDY, a glutaraldehyde cross-linking agent, and an enzyme. Prior to the fabrication, a bare glassy carbon (GC) electrode was polished using a polishing cloth with 0.3 and 0.05 μm alumina slurry and then washed with deionized water followed by sonicating in absolute ethanol and deionized water, respectively. The cleaned electrode was dried under a nitrogen gas flow. NGDY suspension (3 μL) was dropped on a freshly polished GC electrode (denoted as GC/NGDY) surface and allowed to dry at an ambient temperature. Subsequently, 2 μL of the cross-linking agent (0.25% glutaraldehyde), prepared in ultrapure water, was coated onto the modified GC electrode. Finally, the solution of the desired enzyme, 2 μL of AChE or 1 μL of Tyr, was then covered on the electrode (denoted as GC/NGDY/AChE or GC/NGDY/Tyr). The enzyme molecules were entrapped and stabilized on the electrode surface through the cross-linking between the enzyme molecules by glutaraldehyde. The fabricated electrodes were oven-dried for 30 min at 35 °C between steps. The prepared electrodes were stored in a refrigerator at 4 °C when they were not in use.

Scheme 1. Fabrication Process of the Enzyme-Based Biosensor Using NGDY

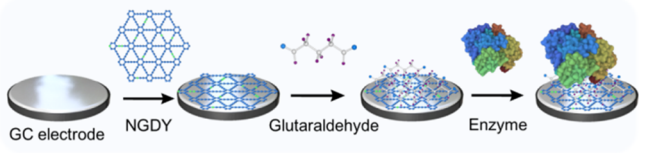

https://doi.org/10.1021/acs.analchem.1c01800
Anal. Chem. 2021, 93, 8656−8662

Electrochemical Measurements. Electrochemical measurements were performed using a CHI 440B electrochemical workstation (Shanghai CH Instruments, China). A GC electrode (diameter of 3 mm), a platinum counter electrode, and a Ag/AgCl reference electrode (3.0 M KCl solution), also obtained from CH Instruments, were used in the electrochemical measurements.

AChE-Based Biosensor for Pesticide Detection. Differential pulse voltammetry (DPV) was conducted to analyze dichlorvos in the potential range of 0.2 to 1.0 V. The performance of biosensors was evaluated by their DPV response in a phosphate buffer solution (PBS, 50 mM, pH 7.4) with 1 mM acetylthiocholine. The modified electrode was immersed into a solution that contains varying amounts of dichlorvos for 15 min. Then, the biosensor was transferred into PBS with 1 mM acetylthiocholine to perform DPV. The inhibition rate ($I\%$) of dichlorvos was calculated using the equation given below:

$$I\% = (I_0 - I_1)/I_0 \times 100\%.$$

where I_0 is the peak current of 1 mM acetylthiocholine in the AChE biosensor and I_1 is the peak current of 1 mM acetylthiocholine in the AChE biosensor after exposure to dichlorvos solution.

Tyr-Based Biosensor for Phenol Detection. The amperometric current−time (i−t) curve for phenol was recorded to comparatively study the properties of various biosensors. A magnetic stirrer was used to support convection in the i−t measurements, which were recorded in PBS (50 mM, pH 6.0). The detection was performed with successive addition of the phenol solution in 5 mL PBS stirred at room temperature.

RESULTS AND DISCUSSION

Characterization of NGDY. NGDY was produced by calcining GDY in an NH_3 atmosphere. The SEM and TEM images of NGDY are shown in Figure 1a and Figure S1, indicating its three-dimensional highly porous nanostructure. Furthermore, the powder XRD pattern (Figure S2) of NGDY shows a wide peak at an angle of 20°, which suggests its amorphous structure. This kind of an open nanostructure significantly increased the effective surface area for enzyme loading and made the substrate more available to enzyme catalysis. Porous structures are also confirmed by the nitrogen adsorption−desorption isotherms (Figure S3). As shown in the pore size distribution curve of Figure S3b, hierarchical microporous and mesoporous structures ranging from 2 to 50 nm were developed in NGDY, which are beneficial for rapid mass transfer of molecules and ions in an aqueous electrolyte. Furthermore, the BET surface area of NGDY is as high as 356 $m^2\ g^{-1}$. The high specific surface area of NGDY provides a large number of anchoring sites for enzyme molecule immobilization.

A Raman spectrum was obtained to characterize NGDY, as shown in Figure 1b. The typical D band and G band can be distinguished easily from the Raman spectrum. In detail, the D band at 1354 cm^{-1} is closely linked to the structural defects, such as disordered carbon atoms and edges and the G band at 1579 cm^{-1} is strongly associated with the first-order scattering of the E2g stretching vibration mode observed for sp^2 carbon domains in aromatic rings. The I_D/I_G ratio of the D band to the G band can be used to determine the defects and disorder of NGDY.[23] The I_D/I_G ratio is almost equal to 0.9, which indicates that NGDY has high structure defects that were produced by N-doping. These structure defects provide plenty of active sites, which are advantageous for improving the sensing performance of the NGDY-based sensors and biosensors. The weak peak at ~2200 cm^{-1} could be due to the vibration of acetylenic chains in NGDY.[20]

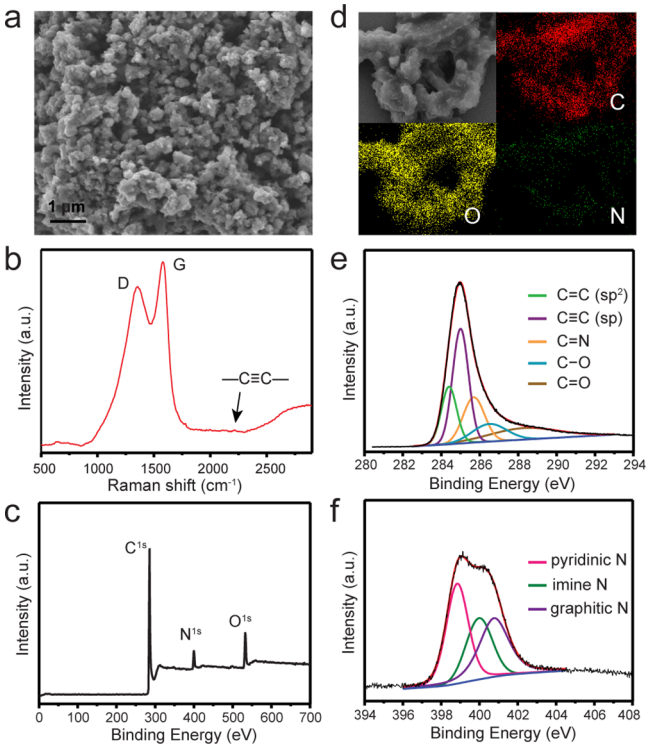

Figure 1. (a) SEM image and (b) Raman spectrum of NGDY. (c) XPS survey spectrum of NGDY. (d) EDS images of NGDY. The images show the elemental mapping analysis of C, N, and O elements of a selected area of NGDY. (e) C 1s spectra of NGDY and (f) N 1s spectra of NGDY.

XPS was further conducted to characterize the surface chemical bonding of NGDY. As shown in Figure 1c, NGDY is mainly composed of elemental C, N, and O, which are found at 285.0, 399.0, and 532.0 eV, respectively. The XPS result, combined with the uniform spatial distribution of C and N atoms in NGDY observed from the elemental mapping (Figure 1d), indicates that the GDY networks have been successfully doped with N. To be more specific, the deconvolution of the C 1s spectrum of NGDY shown in Figure 1e shows five peaks, which correspond to C═C (sp^2) (284.4 eV), C ≡ C (sp) (285.0 eV), C═N (285.6 eV), C−O (286.4 eV), and C═O (288.6 eV) groups.[21,23] A small number of oxygen-containing groups may be assigned to the oxidation of exposed terminal alkynes at the edge of these materials. The high-resolution N 1s peak of NGDY (Figure 1f) shows the fitted characteristic peaks of pyridinic N, imine N, and graphitic N atoms located at 398.8, 399.9, and 400.7 eV, respectively.[26,27] Graphitic N atoms will help to enhance the electrical conductivity of NGDY through the π−π conjugation between the GDY π system and the nitrogen lone-pair electrons. Imine N atoms with a high propensity to accept electrons will produce a net positive charge on the adjacent carbon atoms,[28,29] which are favorable for the adsorption of electron-rich molecules, such as phenol or thiocholine. Hydrogen bonds can be easily formed

https://doi.org/10.1021/acs.analchem.1c01800
Anal. Chem. 2021, 93, 8656−8662

between pyridinic N atoms and phenol or thiocholine within the NGDY layers, thus facilitating the electrochemical reaction.

Electrochemical Characteristics of the AChE-Based Biosensor. To determine the electron transfer ability of NGDY, cyclic voltammetry (CV) was carried out in 1 mM $K_3[Fe(CN)_6]$ containing 0.1 M KCl. As shown in Figure S4, after the modification of NGDY, the electrical conductivity of the bare GC electrode improved evidently. After the immobilization of AChE, a decreased peak current in the CV curve was observed, proving the effective immobilization of the enzyme. AChE immobilized on the bare GC electrode showed the lowest current intensity, also verifying an enhanced electron transfer process caused by NGDY. Benefiting from NGDY with a large surface area and good conductivity, we then prepared a NGDY-based AChE biosensor for OP detection using the enzyme inhibition effect. The inhibition effect of OPs on the GC/NGDY/AChE biosensor is schematically shown in Figure 2a. In this application, AChE

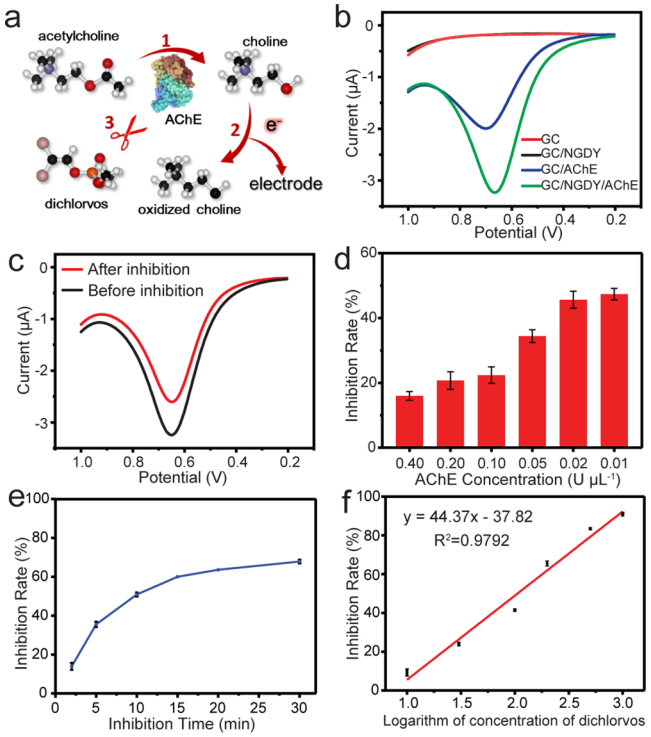

Figure 2. (a) Chemical mechanism of dichlorvos detection by the AChE-based biosensor. (b) DPV curves of different modified electrodes in PBS containing 1 mM acetylthiocholine. (c) DPV curves of the GC/NGDY/AChE electrode containing 0.2 U AChE in 1 mM acetylthiocholine before and after incubation in 100 μg L^{-1} dichlorvos. Parameter optimization for AChE concentration (d) and inhibition time (e) in 1 mM acetylthiocholine under the condition of 100 μg L^{-1} dichlorvos. (f) Calibration curve of dichlorvos detection in a range of 10−1000 μg L^{-1}.

can catalyze acetylthiocholine, an analogue of the neurotransmitter acetylcholine, into acetic acid and thiocholine. Due to the electrochemical activity of thiocholine, it can be oxidized and detected electrochemically. Here, dichlorvos is a common OP, which can inhibit the activity of AChE irreversibly. Therefore, the inhibition percentage can be determined by the inhibition effect based on various dichlorvos concentrations.

As shown in Figure 2b and Figure S5, DPV curves were recorded with or without acetylthiocholine injection to the different modified electrodes. Figure S5 shows that no peak current was observed in all types of electrodes in PBS in the absence of acetylthiocholine. In the presence of acetylthiocholine, still no peak current was observed in GC and GC/NGDY electrodes (Figure 2b), which validates the lack of catalytic activity without AChE. In contrast, the apparent oxidation peak in GC/AChE and GC/NGDY/AChE electrodes can be attributed to the high catalytic power of the enzyme. Compared to the GC/AChE electrode, the voltammetric response peak current of the GC/NGDY/AChE electrode was about twice higher than that of the GC/AChE electrode. This phenomenon should be attributed to NGDY with the main reasons given below. NGDY helps to enhance the conductivity of the biosensor and increase the effective surface area for enzyme loading and substrate reaction. In addition, the pyridinic N within NGDY can form hydrogen bonds with the mercaptan in thiocholine, and the carbon atoms with a net positive charge produced by the imine N atoms will help to adsorb thiocholine, which hasten the electron transfer of thiocholine and increase the oxidation peak currents. It can be concluded that NGDY can help to significantly improve the response signal and sensitivity of this detection system.

Pesticide Detection Using the AChE-Based Biosensor. The inhibition effect of dichlorvos on the AChE-based biosensor was further studied. When dichlorvos was added, the AChE activity was inhibited, resulting in a lower peak current, as shown in Figure 2c. Then the AChE concentration and inhibition time were optimized to improve the performance of the biosensor. As shown in Figure 2d, the rate of inhibition is increased by decreasing the concentration of AChE with a constant acetylthiocholine concentration of 1 mM. Furthermore, the concentration of the enzyme should be selected as the lowest quantity of enzyme capable of generating a measurable signal;[30] thus, 0.02 U was selected as the optimum enzyme concentration. From Figure 2e, it is observed that the inhibition rate continues to increase with increased inhibition time. After 15 min, the inhibition rate almost reaches saturation. Given the short time required for rapid detection, 15 min was chosen as the optimum inhibition time.

Based on the above optimum parameters, DPV was used to monitor the difference among dichlorvos concentrations. The peak currents of GC/NGDY/AChE were reduced with dichlorvos concentrations changing from 10 to 1000 μg L^{-1}, and Figure 2f further shows the linear regression relationship between the inhibition rate and logarithm of concentration of dichlorvos. The limit of detection (LOD) was calculated to be 1.1 μg L^{-1} using the equation LOD = $3\sigma/S$ (σ is the standard deviation of the inhibition rate in the dichlorvos blank and S is the slope of the standard curve).[31] The LOD value of this biosensor is better than those of 22 μg L^{-1} for SiO_2 sol−gel modified screen-printed electrode,[32] 14 μg L^{-1} for mesoporous SiO_2-modified GC electrode,[33] 177 μg L^{-1} for poly(4-aminophenol)-modified graphite electrode,[34] and 172 μg L^{-1} for graphene quantum dot-modified platform.[35]

The repeatability was studied with five independent DPV measurements for one GC/NGDY/AChE biosensor and the relative standard deviation (RSD) was 0.8%, as shown in Figure S6a. The RSD of five individual GC/NGDY/AChE biosensors for 1 mM acetylthiocholine detection was 4.4%, indicating good reproducibility (Figure S6b). The current response of the biosensor decreased to 86% of the initial signal after a storage period of 8 days at 4 °C, showing the long-term stability of the biosensor (Figure S7).

https://doi.org/10.1021/acs.analchem.1c01800
Anal. Chem. 2021, 93, 8656−8662

As shown in Figure 3a, the interference analysis was conducted by recording the DPV signal with and without

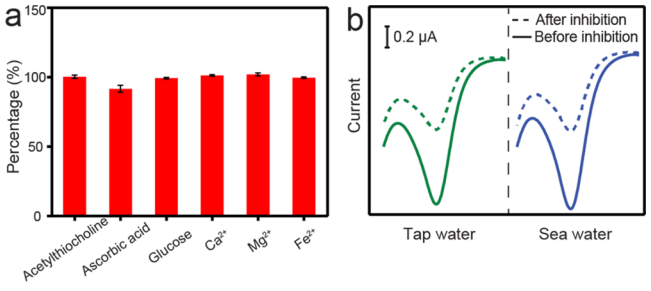

Figure 3. (a) Current response of the as-prepared biosensor in 50 mM PBS (pH 7.4) containing 1 mM acetylthiocholine and 1 mM interferents. (b) Recovery test of 100 μg L^{-1} dichlorvos in tap water and sea water samples.

the inclusion of some potential interferents in 1 mM acetylthiocholine. The electrochemical reaction was rarely influenced in the presence of glucose, Ca^{2+}, Mg^{2+}, Fe^{2+}, etc. In addition, the current changed a little when ascorbic acid was added, owing to the interference by oxidation of ascorbic acid. Since environmental samples generally do not contain ascorbic acid, the interference of ascorbic acid is negligible. To further assess the practical application of this biosensor, the recovery tests of dichlorvos in tap water and sea water were performed, as shown in Figure 3b. The recovery rate of 100 μg L^{-1} dichlorvos in tap water and sea water was 89 and 88%, respectively. The results confirmed the good biosensing performance of this biosensor for the rapid detection of OPs in real environmental samples.

Electrochemical Characteristics of the Tyr-Based Biosensor. The Tyr-based biosensor was used for the detection of phenol. As shown in Figure 4a, three consecutive reactions form the basis of the electrochemical process of this biosensor system. First, in the presence of oxygen and tyrosinase, phenol (C_6H_5OH) was hydroxylated into catechol ($C_6H_6O_2$) followed by the oxidation of catechol into *o*-quinone ($C_6H_4O_2$). Finally, the obtained *o*-quinone was electroreduced to catechol. The electrochemical tyrosinase biosensor is an effective portable instrument for the efficient detection of phenolic contaminants based on the above mechanism. Figure 4b shows the CV curves of GC/NGDY/Tyr in the absence (red line) and presence (black line) of 2 μM phenol in PBS. The reduction peak current significantly improved after injecting phenol, which verifies the successful immobilization of the enzyme on the electrode.

Amperometry was then conducted for phenol detection because of its high sensitivity. Figure 4c shows the comparison of the electrocatalytic ability of different biosensors, and the testing was performed by the successive injection of phenol under constant stirring. Bare GC and GC/NGDY electrodes showed no chronoamperometric responses after the addition of phenol, which validates that tyrosinase is the essential enzyme for the catalytic oxidation. The significant increase in response upon the immobilization of tyrosinase on the electrode confirmed the powerful catalytic ability of the enzyme. Importantly, the sensitivity of GC/NGDY/Tyr was almost 2.5 times higher than that of GC/Tyr in the presence of phenol, which could be ascribed to the following reasons. First, NGDY with a large specific surface area and a highly porous structure (facilitated mass transfer) plays an extremely

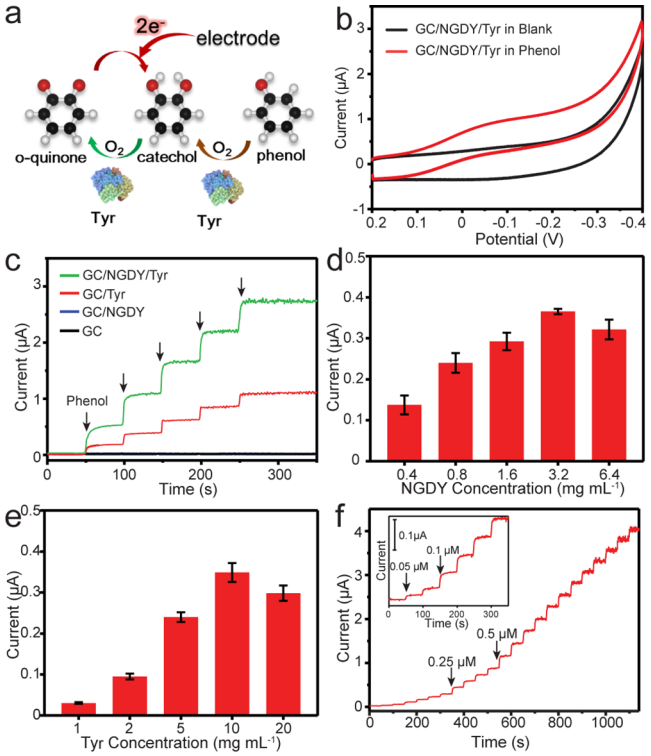

Figure 4. (a) Chemical mechanism of phenol detection by the Tyr-based biosensor. (b) CV curves of the GC/NGDY/Tyr biosensor in the absence and presence of 2 μM phenol. (c) Amperometric current−time response measurements with successive injection of 1 μM phenol on different modified electrodes. Applied potential: −0.15 V vs Ag/AgCl. Effect of optimization of NGDY concentration (d) and Tyr concentration (e) on the amperometric current−time response of the biosensor for the detection of 1 μM phenol. (f) Amperometric current−time response curves of GC/NGDY/Tyr for successive injection of phenol with 0.05, 0.1, 0.25, and 0.5 μM concentrations, respectively.

important role in the improved electrochemical performance. Second, some strong interactions between phenol and NGDY may further expedite the accumulation of phenol on the electrode surface, such as the $\pi-\pi$ interactions between NGDY and the benzene ring of phenol, the hydrogen bond formation between pyridinic N of NGDY and hydroxyl in phenol, and the adsorption interaction between carbonium and phenol. Consequently, NGDY could obviously expedite the catalytic performance of Tyr.

Amperometric Detection of Phenol. Before the chronoamperometric detection of phenol, the experimental conditions such as NGDY concentration (Figure 4d) and Tyr concentration (Figure 4e) were optimized. In brief, with the increase of NGDY and enzyme loading, both the current responses increased as well, ultimately reaching a limit at a particular concentration. Following that, the current responses were both reduced as the NGDY and enzyme loading increased. From the above results, the optimized NGDY concentration and Tyr concentration were chosen as 3.2 and 10 mg mL^{-1}, respectively. As shown in Figure 4f, the amperometric detection of phenol was carried out with the addition of different phenol concentrations based on the optimized parameters. Results showed that the current response has a linear correlation with the phenol concentration in the range from 0.02 to 5 μM with R^2 = 0.9998 (Figure S8).

https://doi.org/10.1021/acs.analchem.1c01800
Anal. Chem. 2021, 93, 8656−8662

In addition, the LOD of this biosensor was calculated to be about 5.8 nM (signal-to-noise ratio equals 3), which is significantly better than that of other nanomaterial-modified tyrosinase electrodes, such as CNTs (130 nM),[36] 2D pnictogens (225 nM),[11] mesoporous carbon (20 nM),[37] and MXenes (12 nM).[38]

The good repeatability of the GC/NGDY/AChE biosensor was demonstrated by successive determination of 1 μM phenol for five times with an RSD of 2.9% (Figure S9a). The reproducibility of the GC/NGDY/Tyr biosensor was studied by assaying three individual biosensors for 1 μM phenol detection and the RSD was determined to be 3.4%, indicating the good reproducibility of the biosensor (Figure S9b). The GC/NGDY/Tyr biosensor can maintain 85% of its original response after 8 days of storage at 4 °C, showing acceptable stability (Figure S10).

Some typical interfering species were chosen to measure the interference tolerance of the biosensor. As shown in Figure 5a,

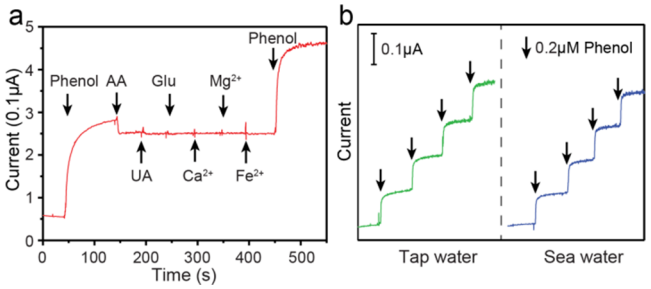

Figure 5. (a) Chronoamperometry responses of the biosensor in the presence of 1 μM phenol and its common interfering species, such as 20 μM ascorbic acid (AA), 20 μM uric acid (UA), 20 μM glucose (Glu), 20 μM Ca^{2+}, 20 μM Mg^{2+}, and 20 μM Fe^{2+}. (b) Recovery experiments performed by adding 0.2 μM phenol into tap water and sea water samples.

there is no significant change in the current response when adding 20 times concentration (20 μM) of UA, Glu, Ca^{2+}, Mg^{2+}, and Fe^{2+} in 1 μM phenol. Based on the reaction mechanism, the current response of phenol detection by the Tyr-based biosensor was produced by the electrochemical reduction of *o*-quinone. AA can chemically reduce *o*-quinone, which can lead to a lower concentration of *o*-quinone. Thus, the addition of AA can generate a little current response decrease.[39,40] To evaluate the applicability of this fabricated biosensor in real environmental samples, the recovery experiments were conducted by testing tap water and sea water spiked with phenol, as shown in Figure 5b The recoveries for tap water and sea water spiked with 0.2 μM phenol were calculated to be 102 and 94%, respectively. The typical ions in the seawater sample have been analyzed by inductively coupled plasma–atomic emission spectroscopy and ion chromatography, and the result shows that the sample contains mainly about 469 mM Na^+, 53 mM Mg^{2+}, 10 mM K^+, 431 mM Cl^-, and 2 mM NO_3^-.[41,42] All these results reveal that the as-fabricated biosensor is a reliable tool for the rapid and efficient detection of phenol in real water samples.

CONCLUSIONS

In this work, NGDY was produced by calcining GDY in an NH_3 atmosphere, and an AChE-based pesticide biosensor and a Tyr-based phenol biosensor were successfully prepared by applying NGDY as the biosensing platform. The obtained NGDY exhibits a large surface area, a hierarchical nanoporous structure, high structure defects, and good conductivity, which are beneficial for enzyme immobilization, substance diffusion, and electron transport. Results demonstrate that these two types of enzymatic electrochemical biosensors show significantly improved sensitivity, excellent reproducibility, good stability, and an acceptable recovery rate, which make them a powerful tool to be applied for the rapid detection of OPs and phenols in the environment. The different kinds of N atoms (graphitic N, imine N, and pyridinic N) in NGDY are believed to play a key role in enhancing the performance of biosensors. By exploring two completely different biosensors with excellent performance, for the first time, this study proves that NGDY can be used as a robust biosensing platform for the development of different kinds of biosensors and has broad application prospects.

ASSOCIATED CONTENT

Supporting Information

The Supporting Information is available free of charge at https://pubs.acs.org/doi/10.1021/acs.analchem.1c01800.

TEM, XRD spectra and nitrogen adsorption–desorption isotherms of NGDY, CV curves of different modified electrodes in 1.0 mM $K_3[Fe(CN)_6]$ solution, DPV curves of different modified electrodes in PBS, calibration curve of phenol detection, repeatability, reproducibility, and stability test of two types of biosensors (PDF)

AUTHOR INFORMATION

Corresponding Author

Xianbo Lu − *CAS Key Laboratory of Separation Science for Analytical Chemistry, Dalian Institute of Chemical Physics, Chinese Academy of Sciences, Dalian, Liaoning 116023, P. R. China*; orcid.org/0000-0003-3983-7812; Email: xianbolu@dicp.ac.cn

Authors

Kai Niu − *CAS Key Laboratory of Separation Science for Analytical Chemistry, Dalian Institute of Chemical Physics, Chinese Academy of Sciences, Dalian, Liaoning 116023, P. R. China; University of Chinese Academy of Sciences, Beijing 100049, P. R. China*

Juan Gao − *School of Chemistry and Chemical Engineering, Beijing Institute of Technology, Beijing 100081, P. R. China*

Lingxia Wu − *CAS Key Laboratory of Separation Science for Analytical Chemistry, Dalian Institute of Chemical Physics, Chinese Academy of Sciences, Dalian, Liaoning 116023, P. R. China*

Jiping Chen − *CAS Key Laboratory of Separation Science for Analytical Chemistry, Dalian Institute of Chemical Physics, Chinese Academy of Sciences, Dalian, Liaoning 116023, P. R. China*; orcid.org/0000-0001-9404-1687

Complete contact information is available at: https://pubs.acs.org/10.1021/acs.analchem.1c01800

Author Contributions

K.N. and J.G. contributed equally to this work. K.N. and X.L. conceived the idea and designed this research study. J.G. prepared NGDY and recorded the powder XRD spectra and nitrogen adsorption–desorption isotherms of NGDY. K.N. performed the rest of the experiments. K.N., J.G., and L.W.

https://doi.org/10.1021/acs.analchem.1c01800
Anal. Chem. 2021, 93, 8656–8662

analyzed the data. K.N., X.L., and J.C. wrote the manuscript. All authors have given approval to the final version of the manuscript.

Notes

The authors declare no competing financial interest.

■ ACKNOWLEDGMENTS

This work was financially supported by the National Natural Science Foundation of China (Grant No. 22076181), the Dalian Science and Technology Innovation Fund (2020JJ26SN057), DICP I202001, and the Natural Science Foundation of Liaoning Province (2019-MS-317).

■ REFERENCES

(1) Tang, W.; Yang, J.; Wang, F.; Wang, J.; Li, Z. *Anal. Chim. Acta* **2019**, *1060*, 97−102.
(2) Lu, R.; Li, W. W.; Mizaikoff, B.; Katzir, A.; Raichlin, Y.; Sheng, G. P.; Yu, H. Q. *Nat. Protoc.* **2016**, *11*, 377−386.
(3) Mei, L. P.; Feng, J. J.; Wu, L.; Zhou, J. Y.; Chen, J. R.; Wang, A. J. *Biosens. Bioelectron.* **2015**, *74*, 347−352.
(4) Li, H.; Yang, J.; Gao, M.; Wang, J.; Sun, B. *Food Chem.* **2019**, *271*, 388−392.
(5) Correia-Sá, L.; Norberto, S.; Delerue-Matos, C.; Calhau, C.; Domingues, V. F. *J. Chromatogr. B Analyt. Technol. Biomed. Life. Sci.* **2018**, *1072*, 9−16.
(6) Wang, J.; Gong, Z.; Zhang, T.; Feng, S.; Wang, J.; Zhang, Y. *J. Sep. Sci.* **2017**, *40*, 2398−2405.
(7) Cui, H. F.; Wu, W. W.; Li, M. M.; Song, X. J.; Lv, Y. X.; Zhang, T. T. *Biosens. Bioelectron.* **2018**, *99*, 223−229.
(8) Zhang, Y.; Pan, D.; Zhou, Q.; Zhao, J.; Pan, N.; Zhang, Y.; Wang, L. X.; Shen, Y. *J. Mater. Chem. B* **2018**, *6*, 8180−8187.
(9) Zhao, F.; Yao, Y.; Li, X.; Lan, L.; Jiang, C.; Ping, J. *Anal. Chem.* **2018**, *90*, 11658−11664.
(10) Zhao, F.; Yao, Y.; Jiang, C.; Shao, Y.; Barcelo, D.; Ying, Y.; Ping, J. *J. Hazard. Mater.* **2020**, *384*, No. 121358.
(11) Mayorga-Martinez, C. C.; Gusmão, R.; Sofer, Z.; Pumera, M. *Angew. Chem., Int. Ed.* **2019**, *58*, 134−138.
(12) Wu, L.; Gao, J.; Lu, X.; Huang, C.; Dhanjai; Chen, J. P. *Carbon* **2020**, *156*, 568−575.
(13) Guo, S. Y.; Yan, H. L.; Wu, F.; Zhao, L. J.; Yu, P.; Liu, H. B.; Li, Y. L.; Mao, L. Q. *Anal. Chem.* **2017**, *89*, 13008−13015.
(14) Jia, Z.; Li, Y.; Zuo, Z.; Liu, H.; Huang, C.; Li, Y. *Acc. Chem. Res.* **2017**, *50*, 2470−2478.
(15) Yu, H.; Hui, L.; Xue, Y.; Liu, Y.; Fang, Y.; Xing, C.; Zhang, C.; Zhang, D.; Chen, X.; Du, Y.; Wang, Z.; Gao, Y.; Huang, B.; Li, Y. *Nano Energy* **2020**, *72*, No. 104667.
(16) Parvin, N.; Jin, Q.; Wei, Y. Z.; Yu, R. B.; Zheng, B.; Huang, L.; Zhang, Y.; Wang, L. H.; Zhang, H.; Gao, M. Y.; Zhao, H. J.; Hu, W. P.; Li, Y. L.; Wang, D. *Adv. Mater.* **2017**, *29*, 7.
(17) Li, J.; Jiu, T.; Chen, S.; Liu, L.; Yao, Q.; Bi, F.; Zhao, C.; Wang, Z.; Zhao, M.; Zhang, G.; Xue, Y.; Lu, F.; Li, Y. *Nano Lett.* **2018**, *18*, 6941−6947.
(18) Lv, Q.; Si, W. Y.; He, J. J.; Sun, L.; Zhang, C. F.; Wang, N.; Yang, Z.; Li, X. D.; Wang, X.; Deng, W. Q.; Long, Y. Z.; Huang, C. S.; Li, Y. L. *Nat. Commun.* **2018**, *9*, 11.
(19) Zhao, Y.; Yang, N.; Yao, H.; Liu, D.; Song, L.; Zhu, J.; Li, S.; Gu, L.; Lin, K.; Wang, D. *J. Am. Chem. Soc.* **2019**, *141*, 7240−7244.
(20) Zhao, Y.; Wan, J.; Yao, H.; Zhang, L.; Lin, K.; Wang, L.; Yang, N.; Liu, D.; Song, L.; Zhu, J.; Gu, L.; Liu, L.; Zhao, H.; Li, Y.; Wang, D. *Nat. Chem.* **2018**, *10*, 924−931.
(21) Lv, Q.; Si, W.; Yang, Z.; Wang, N.; Tu, Z.; Yi, Y.; Huang, C.; Jiang, L.; Zhang, M.; He, J.; Long, Y. *ACS Appl. Mater. Interfaces* **2017**, *9*, 29744−29752.
(22) Gao, L.; Ge, X.; Zuo, Z.; Wang, F.; Liu, X.; Lv, M.; Shi, S.; Xu, L.; Liu, T.; Zhou, Q.; Ye, X.; Xiao, S. *Nano Lett.* **2020**, *20*, 7333−7341.
(23) Zhang, S.; Du, H.; He, J.; Huang, C.; Liu, H.; Cui, G.; Li, Y. *ACS Appl. Mater. Interfaces* **2016**, *8*, 8467−8473.
(24) Xu, H.; Liao, C.; Liu, Y.; Ye, B.-C.; Liu, B. *Anal. Chem.* **2018**, *90*, 4438−4444.
(25) Li, G.; Li, Y.; Liu, H.; Guo, Y.; Li, Y.; Zhu, D. *Chem. Commun.* **2010**, *46*, 3256−3258.
(26) Si, W.; Yang, Z.; Wang, X.; Lv, Q.; Zhao, F.; Li, X.; He, J.; Long, Y.; Gao, J.; Huang, C. *ChemSusChem* **2019**, *12*, 173−178.
(27) Yang, C. F.; Qiao, C.; Chen, Y.; Zhao, X. Q.; Wu, L. L.; Li, Y.; Jia, Y.; Wang, S. Y.; Cui, X. L. *Small* **2020**, *16*, 11.
(28) Gu, J. X.; Magagula, S.; Zhao, J. X.; Chen, Z. F. *Small Methods* **2019**, *3*, 8.
(29) Chen, X. Z.; Ong, W. J.; Kong, Z. Z.; Zhao, X. J.; Li, N. *Sci. Bull.* **2020**, *65*, 45−54.
(30) Nasir, M. Z. M.; Mayorga-Martinez, C. C.; Sofer, Z.; Pumera, M. *ACS Nano* **2017**, *11*, 5774−5784.
(31) Memon, A. G.; Xing, Y. P.; Zhou, X. H.; Wang, R. Y.; Liu, L. H.; Zeng, S. Y.; He, M.; Ma, M. *J. Hazard. Mater.* **2020**, *384*, 6.
(32) Sotiropoulou, S.; Chaniotakis, N. A. *Biomaterials* **2005**, *26*, 6771−6779.
(33) Itoh, T.; Shimomura, T.; Hayashi, A.; Yamaguchi, A.; Teramae, N.; Ono, M.; Tsunoda, T.; Mizukami, F.; Stucky, G. D.; Hanaoka, T. A. *Analyst* **2014**, *139*, 4654−4660.
(34) Melo, E. I.; Franco, D. L.; Afonso, A. S.; Rezende, H. C.; Brito-Madurro, A. G.; Madurro, J. M.; Coelho, N. M. M. *Braz. Arch. Biol. Technol.* **2011**, *54*, 1217−1222.
(35) Sahub, C.; Tuntulani, T.; Nhujak, T.; Tomapatanaget, B. *Sens. Actuators B Chem.* **2018**, *258*, 88−97.
(36) Caetano, F. R.; Carneiro, E. A.; Agustini, D.; Figueiredo-Filho, L. C. S.; Banks, C. E.; Bergamini, M. F.; Marcolino-Junior, L. H. *Biosens. Bioelectron.* **2018**, *99*, 382−388.
(37) Wu, L.; Lu, X.; Zhang, H.; Chen, J. *ChemSusChem* **2012**, *5*, 1918−1925.
(38) Wu, L.; Lu, X.; Dhanjai; Wu, Z.; Dong, Y.; Wang, X.; Zheng, S.; Chen, J. *Biosens. Bioelectron.* **2018**, *107*, 69−75.
(39) Sima, V. H.; Patris, S.; Aydogmus, Z.; Sarakbi, A.; Sandulescu, R.; Kauffmann, J. M. *Talanta* **2011**, *83*, 980−987.
(40) Taira, N.; Katsuyama, Y.; Yoshioka, M.; Muraoka, O.; Morikawa, T. *Int. J. Mol. Sci.* **2018**, *19*, 22.
(41) Besson, P.; Degboe, J.; Berge, B.; Chavagnac, V.; Fabre, S.; Berger, G. *Geostand. Geoanal. Res.* **2014**, *38*, 355−362.
(42) Rodrigues, J.; da Silva, R.; Camões, M. F. G. F. C.; Oliveira, C. M.; Oliveira, C. M. *Talanta* **2015**, *142*, 72−83.

https://doi.org/10.1021/acs.analchem.1c01800
Anal. Chem. 2021, 93, 8656−8662